

Avalanches, irreversibility, and phase separation in Co-substituted $\text{Pr}_{0.50}\text{Ca}_{0.50}\text{Mn}_{1-x}\text{Co}_x\text{O}_3$ C. Yaicle,¹ C. Frontera,² J. L. García-Muñoz,² C. Martin,¹ A. Maignan,¹ G. André,³ F. Bourée,³ C. Ritter,⁴ and I. Margiolaki⁵¹Laboratoire CRISMAT, UMR 6508 CNRS/Ensicaen, 6 bd du Maréchal Juin, F-14050 Caen Cedex, France²Institut de Ciència de Materials de Barcelona, CSIC, Campus Universitari de Bellaterra, E-08193 Bellaterra, Spain³LLB, CEA-Saclay, F-91191 Gif-Sur-Yvette Cedex, France⁴Institut Laue Langevin, Boîte Postale 156, F-38042 Grenoble Cedex 9, France⁵European Synchrotron Radiation Facility, ESRF, Boîte Postale 220, F-38043 Grenoble, France

(Received 5 May 2006; revised manuscript received 17 July 2006; published 6 October 2006)

Combining magnetization and magnetotransport measurements, synchrotron, and neutron powder diffraction data, we have deeply studied the structural and magnetic nature of segregated phases, and the occurrence of magnetization and resistivity avalanches under magnetic field in $\text{Pr}_{0.50}\text{Ca}_{0.50}\text{Mn}_{1-x}\text{Co}_x\text{O}_3$ ($x=0.02$ and 0.05). We report the segregation of two phases at low temperature which evolve with Co content. For $x=0.05$ these phases (82 wt. % and 18 wt. %) present different distortion degrees, and different strain. The less distorted (and more strained) being ferromagnetically ordered and the more distorted being magnetically disordered. For $x=0.02$ both phases (58 wt. % and 42 wt. %) are highly and similarly distorted, and exhibit CE-type antiferromagnetic order. We find that spontaneous phase segregation occurs independently of the formation of ferromagnetic regions, and report the absence of pseudo-CE phase in these Co substituted manganites. In addition, low temperature magnetization vs field curves present a highly irreversible behavior (after the first magnetization curve): the occurrence of magnetization steps is a manifestation of the irreversible effect of magnetic field at low temperature, but this irreversibility is independent of the occurrence of steps. The evolution of internal strains is analyzed under Co substitution.

DOI: [10.1103/PhysRevB.74.144406](https://doi.org/10.1103/PhysRevB.74.144406)

PACS number(s): 75.25.+z, 71.30.+h, 71.38.-k, 71.45.Lr

I. INTRODUCTION

Phase segregation phenomena have become nowadays an important area of research due to their crucial role in some of the most relevant properties of transition metal oxides such as high-temperature superconductivity¹ or colossal magnetoresistance (CMR).² In particular, static or dynamic phase separation phenomena are at the origin of the unconventional magnetic and transport properties of the perovskite-based CMR manganites. The terms “charge ordered” (CO) and “charge disordered” (CD) are frequently used when referring to the insulating and metallic phases in $\text{Ln}_{1-x}\text{Ca}_x\text{MnO}_3$ compounds. Although the charge order state is the common state found in half-doped manganites such as $\text{Pr}_{0.5}\text{Ca}_{0.5}\text{MnO}_3$, the nature of the CO phase is still the subject of debate. CO was initially understood as a pure ionic arrangement of $\text{Mn}^{3+}/\text{Mn}^{4+}$ ions in the lattice,^{3,4} accompanied by an ordered occupation of the e_g orbitals (orbital order, OO). However, diffraction data on these systems do not support the ionic description,⁵⁻⁷ and different alternative scenarios have been proposed, based on a partial charge disproportionation,⁸ the ordered condensation of Zener polarons (ZP) (Ref. 9) or charge density waves.¹⁰

Other manifestations of the rich and complex properties of simple Mn perovskites are the properties displayed under the substitution of Mn by a few percent of other cations in polycrystalline $\text{Pr}_{0.5}\text{Ca}_{0.5}\text{MnO}_3$ samples.¹¹⁻¹⁸ To be highlighted are (i) the loss of charge ordering and the formation of a metallic and conducting phase at very low substitution levels (3%–5%);¹¹⁻¹³ and (ii) the observation of steplike metamagnetic transitions under applied magnetic field in different $\text{Pr}_{0.5}\text{Ca}_{0.5}\text{Mn}_{1-x}\text{M}_x\text{O}_3$ ($M=\text{Co}, \text{Ga}, \text{Ni}, \dots$) compounds.¹⁴⁻¹⁸ Some structural studies have revealed that

these compounds present a separation between two different phases of a different nature. It has been suggested that the nature of these phases as well as the macroscopic behavior of the substituted manganite depends on the electronic structure of the substituting ions:¹⁵ M cations with unpaired d electrons would favor the stabilization of FM-metallic islands or regions in the AFM-insulating (and CO) matrix, in contrast to M cations having empty or closed d shells.¹⁷ The coexistence of different crystalline phases is accompanied by the coexistence of different long range magnetic arrangements. In this sense, two different cases have been reported. When FM is favored (active d electrons), it is accompanied by long range CE and pseudo-CE (Refs. 3 and 4) magnetic order,¹⁸ when FM is not favored (no active d electrons), both CE and pseudo-CE regions are present.^{12,13,17} Generally, the phase giving pseudo-CE magnetic ordering is less stable, under the application of a magnetic field, than the CE-type magnetic domains. This supports the idea that magnetization avalanches start preferentially at pseudo-CE regions. Consistently, neutron studies under field indicate that the pseudo-CE order disappears more quickly than the CE order.¹⁷

In Ref. 15 detailed magnetic, resistivity, and magnetotransport measurements performed on a polycrystalline sample of $\text{Pr}_{0.5}\text{Ca}_{0.5}\text{Mn}_{0.95}\text{Co}_{0.05}\text{O}_3$ demonstrated the unconventional features of the steplike metamagnetic transitions. Although the origin of these steps is still not well understood, the “critical fields” were found to vary linearly with the cooling field applied to the sample.¹⁵ One should in consequence not use the term critical fields since both the amplitude of the avalanches and the transition fields depend on the field variation rate. On the other hand, the avalanches have been confirmed to be an intrinsic property at low temperatures, observable in both polycrystalline and single crys-

tal samples. The magnetization and resistivity steps have been interpreted as a result of the competition between the magnetic and magnetocaloric energies promoting the FM and the elastic energy associated with the strains at the interfaces between the domains of different phases related by a martensitic transformation.

In this paper we examine these phenomena in $\text{Pr}_{0.5}\text{Ca}_{0.5}\text{Mn}_{1-x}\text{Co}_x\text{O}_3$ (with $x=0.02$ and 0.05), putting special emphasis to two aspects: (i) understanding the macroscopic response from a proper knowledge of the electronic/magnetic/structural inhomogeneities at a microscopic level; and (ii) understanding the evolution with the substitution level x of the physical properties of separated phases. The system chosen is very appropriate for the later because, as we will show, great changes in the microscopic and macroscopic physical properties take place with small differences in the substitution level.

II. EXPERIMENTAL DETAILS

Polycrystalline $\text{Pr}_{0.5}\text{Ca}_{0.5}\text{Mn}_{1-x}\text{Co}_x\text{O}_3$ ($x=0.02$ and 0.05) ceramics were prepared as bars and powders by standard solid state ceramic synthesis in air. Stoichiometric mixtures of the oxides Pr_6O_{11} , CaO , MnO_2 , and Co_3O_4 were intimately ground, heated first at 1000°C and then pressed in the form of bars. After some intermediate treatments, the final annealing temperatures of the bars were 1200°C and 1500°C . The samples were slowly cooled down to 800°C (100°C/h), and then quenched to room temperature. Bars were cut in several pieces of different size for characterization using different techniques. Laboratory x-ray diffraction indicated single phased orthorhombic $\sqrt{2}a_p \times 2a_p \times \sqrt{2}a_p$ structure ($Pnma$). A minor side phase, Mn_3O_4 , was detected [weight ratio $\approx 1.9(5)\%$] and accounted for appropriately.

Neutron powder diffraction (NPD) patterns were collected at the Laboratoire Leon-Brillouin (LLB, Saclay, France) and the Institut Laue-Langevin (ILL, Grenoble). For $\text{Pr}_{0.5}\text{Ca}_{0.5}\text{Mn}_{0.95}\text{Co}_{0.05}\text{O}_3$ (hereafter Co-5%) we recorded high-resolution data at room temperature (RT) and 10 K using the 3T-2 diffractometer ($\lambda=1.225\text{ \AA}$, LLB). The medium resolution G4-1 diffractometer ($\lambda=2.426\text{ \AA}$, LLB) was also used to collect data between 1.5 K and 300 K in 5 K incremental steps. For $\text{Pr}_{0.5}\text{Ca}_{0.5}\text{Mn}_{0.98}\text{Co}_{0.02}\text{O}_3$ (hereafter Co-2%), NPD data were collected on the high resolution D2B ($\lambda=1.594\text{ \AA}$) diffractometer at ILL-Grenoble, at 3, 90, 150 K, and RT.

Synchrotron x-ray powder diffraction (SPD) patterns for both samples were also collected at the ultrahigh resolution diffractometer ID31 ($\lambda=0.429\,697\text{ \AA}$) of the ESRF (Grenoble, France). The short wavelength, to reduce the absorption, was selected with a double-crystal Ge (111) monochromator and calibrated with Si NIST ($a=5.430\,94\text{ \AA}$). Optimum transmission was achieved by enclosing the finely ground sample in a 0.5 mm diameter borosilicate glass capillary, and appropriate spinning of the capillary in the beam ensured for a good powder averaging. Low temperature patterns were recorded placing the capillary in a continuous liquid-helium flow cryostat with rotating sample rod. All diffraction data were analyzed by the Rietveld method using the

FullProf package.¹⁹ In order to obtain reliable microstructural informations on the measured samples, we have first determined the contribution to the profile shape function coming from the diffractometer. This has been achieved by measuring well crystallized $\text{Na}_2\text{Ca}_3\text{Al}_2\text{F}_{14}$, with a negligible sample contribution.²⁰ The contribution coming from the samples has been analyzed following the Stephens' formalism implemented in the FullProf 2000 program.²¹ According to this formulation, the contribution to the broadening of (hkl) reflection due to the strain reads

$$\sigma_{hkl}^2 = \sum_{\substack{H,K,L \\ H+K+L=4}} S_{HKL} h^H k^K l^L, \quad (1)$$

where S_{HKL} are refinable parameters related to the fluctuation of distances between crystallographic planes. For an orthorhombic cell, only six terms of this sum are different from zero

$$\sigma_{hkl}^2 = S_{400}h^4 + S_{040}k^4 + S_{004}l^4 + S_{220}h^2k^2 + S_{202}h^2l^2 + S_{022}k^2l^2. \quad (2)$$

Magnetization measurements were performed using a SQUID magnetometer (Quantum Design), ac susceptibility and magnetotransport data (by the four-probe method) were recorded using a commercial PPMS system (Quantum Design) in the temperature range $2 < T < 350\text{ K}$.

III. RESULTS AND DISCUSSION

A. Magnetic and magnetotransport measurements

Figure 1(a) presents the magnetization curve of the Co-5% compound, measured with an applied field of 0.2 and 1.45 T. The sudden increase, on cooling, displayed by these curves at $T_C \approx 80\text{ K}$ evidences the appearance of long range ferromagnetic order at this temperature. These data are consistent with the evolution of the ordered magnetic moment of the Mn site obtained from NPD data [Fig. 1(b)] as we will discuss in the next section, and are consistent with previously published data on the same compound.¹⁵ Figure 1(a) also plots the inverse dc susceptibility (measured under 0.2 and 1.45 T) of the Co-5% sample. These data show a clear anomaly at about 200 K, in the paramagnetic region. Such anomalies are usually found in half doped manganites at the CO transition, so we identify this anomaly as a signal of this ordering taking place at $T_{CO} \approx 200\text{ K}$. Magnetization (measured under 0.2 T) and the ordered magnetic moment found by NPD show a diminution (on cooling) that takes place at about 40 K. This diminution is present in other Pr containing manganites (such as $\text{Pr}_{0.7}\text{Ca}_{0.3}\text{MnO}_3$) and is usually interpreted in terms of a polarization of the Pr ions.²² Figure 2 presents the resistivity of this compound measured at zero field and with an applied field of 7.5 T. The paramagnetic to ferromagnetic transition present in the magnetic data is clearly reflected in these transport data as an insulator ($T > T_C$) to metal ($T < T_C$) transition, accompanied by strong magnetoresistance as is usually found in manganites. It is worth mentioning that at 200 K, when the CO transition is seen in susceptibility data, no special feature can be appre-

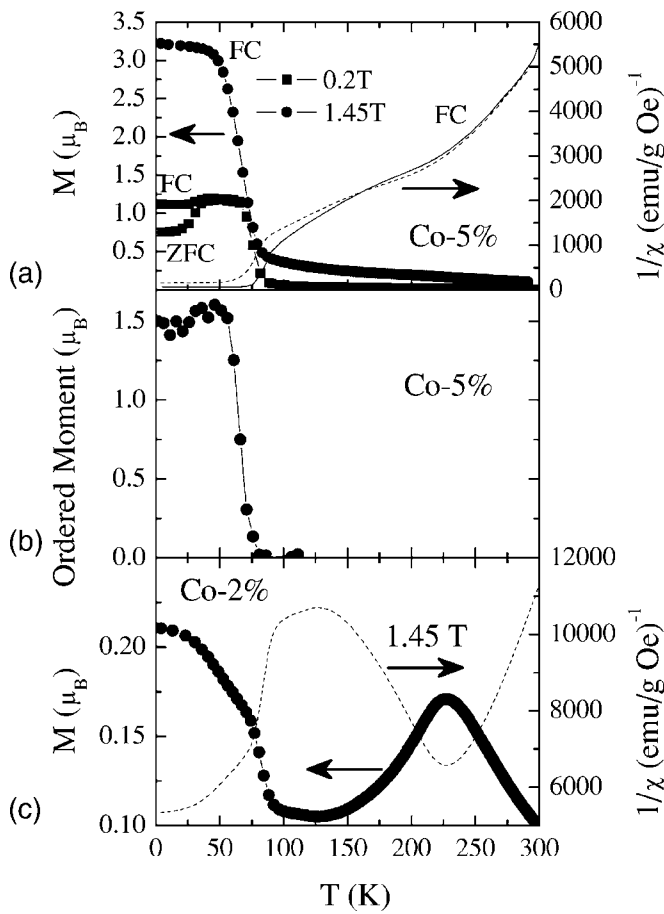


FIG. 1. (a) left axis: Temperature dependence of the magnetization per f.u. of $\text{Pr}_{0.50}\text{Ca}_{0.50}\text{Mn}_{0.95}\text{Co}_{0.05}\text{O}_3$ measured under 0.2 T (squares, FC, and ZFC) and under 1.45 T (circles, FC). (a) right axis: Inverse dc susceptibility of $\text{Pr}_{0.50}\text{Ca}_{0.50}\text{Mn}_{0.95}\text{Co}_{0.05}\text{O}_3$ obtained after FC under 0.2 T (solid line) and 1.45 T (dashed line). (b) Evolution of the ordered ferromagnetic moment per Mn site refined from NPD data as a function of temperature for $\text{Pr}_{0.50}\text{Ca}_{0.50}\text{Mn}_{0.95}\text{Co}_{0.05}\text{O}_3$ (neutrons) (c) left axis: Temperature dependence of the magnetization per f.u. of $\text{Pr}_{0.50}\text{Ca}_{0.50}\text{Mn}_{0.98}\text{Co}_{0.02}\text{O}_3$ measured under 1.45 T after FC. (c) right axis: Corresponding reciprocal dc susceptibility of $\text{Pr}_{0.50}\text{Ca}_{0.50}\text{Mn}_{0.98}\text{Co}_{0.02}\text{O}_3$ obtained after FC under 1.45 T.

ciated even when resistivity derivatives and/or the activation energy are carefully examined. On the other hand, there is a clearly visible anomaly in the $\rho(T)$ curve below the Curie temperature, at about 50 K. Such a second anomaly can also be seen in the $\rho(T)$ curve measured with an applied field of 7.5 T at about 25 K below the maximum. This anomaly cannot be related to the diminution of the magnetic moment (on cooling) at about 40 K, as it happens clearly above this temperature.

Figure 1(c) shows the magnetization of Co-2% measured under 1.45 T of applied field (field cooled), together with its inverse dc susceptibility. According to these measurements, a small but clear FM component appears at $T_C \approx 80$ K. This component is much smaller than that detected in the Co-5% compound, but the temperature where it appears is the same. The appearance of CO at $T_{CO} \approx 225$ K is clearly seen as an anomaly in the inverse susceptibility and a maxi-

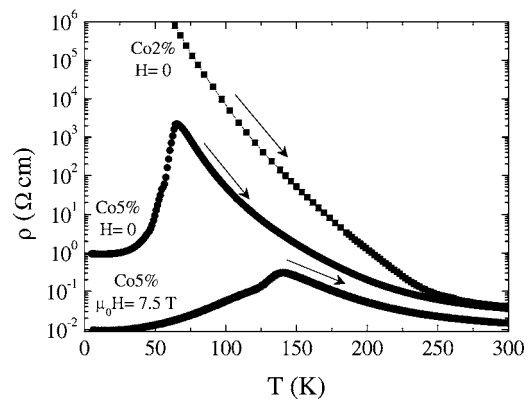


FIG. 2. Resistivity of $\text{Pr}_{0.50}\text{Ca}_{0.50}\text{Mn}_{0.95}\text{Co}_{0.05}\text{O}_3$ (measured at zero field and at 7.5 T, as labeled) and $\text{Pr}_{0.50}\text{Ca}_{0.50}\text{Mn}_{0.98}\text{Co}_{0.02}\text{O}_3$ samples as a function of temperature measured on heating.

mum of the magnetization data. The CO transition can also be clearly appreciated in the resistivity data, shown in Fig. 2, presenting a change of slope at this temperature. Below 225 K the resistivity grows rapidly on cooling and becomes too large to be measured below ~ 60 K. Although magnetization data signals the appearance of a very tiny FM component (under 1.45 T), this compound remains insulating in zero field. From the value of the low temperature magnetization in Fig. 1(c), the fraction of FM phase is below $\sim 6\%$. This value does not allow metallic domains to percolate the system.

For further characterizing these compounds, we have also measured the isothermal magnetization and resistivity curves under applied field. Figure 3(a) shows the magnetization vs field curves of Co-2%, Co-5%, and, for comparison, of the parent $\text{Pr}_{0.5}\text{Ca}_{0.5}\text{MnO}_3$ compound. The last one shows a monotonous and small enhancement of the magnetization up to 5 T with the process being completely reversible when releasing the field. On the contrary, the magnetization curves of Co-2% and Co-5% present a different steplike enhancement when applying the magnetic field and a remarkably hysteretic behavior when releasing the field. From the $M(H)$ curve of Co-2%, it is evident that no spontaneous magnetization appears after a ZFC process. This means that the small magnetization shown in Fig. 1(c) is not spontaneous but due to the field cooling process. The measured isothermal resistivity under field is shown in the inset of Fig. 3(a) for Co-2% and Co-5%. The resistivity of Co-5% presents different steps during the sweep up of the magnetic field, corresponding to the different steps of the magnetization (a direct correlation between the two curves cannot be established due to the fact that both measurements were done on different pieces of the material). The high value of the resistance of Co-2% prevented us from measuring the resistivity at low temperature and low fields (before increasing the field). A quick drop when applied field is found near 10 T, which must correspond to a large magnetization change, afterwards, when releasing the field, the resistivity grows up a little presenting a huge hysteresis.

From this figure it becomes clear that the magnetic field induces some irreversible transition in substituted compounds at low temperature. Further insight in this behavior is

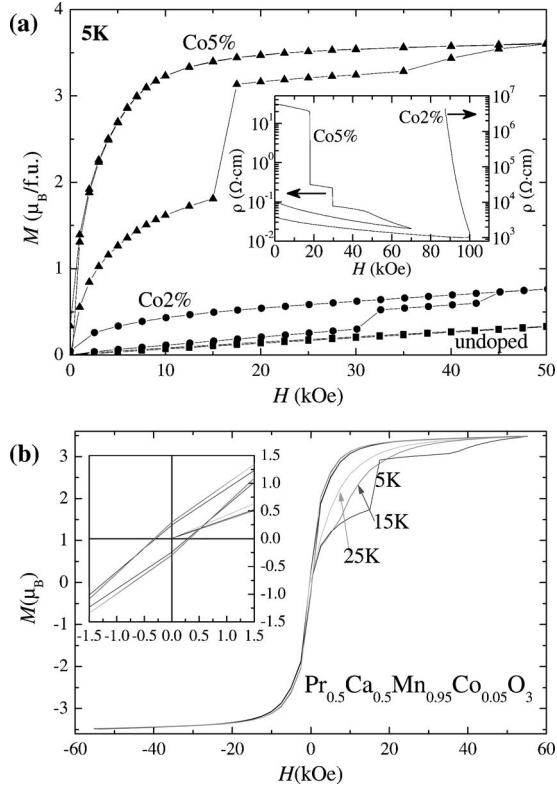


FIG. 3. (a) Isothermal magnetization vs field obtained at 5 K of Co-5% (triangles), Co-2% (circles) and parent (squares) compounds. (Inset) resistivity vs field for Co-2% and Co-5% compounds. (b) Complete isotherm magnetization loop for Co-5% at different temperatures from 5 to 25 K. The inset shows in detail the middle part of the hysteresis loop.

obtained by examining data presented in Fig. 3(b). This figure shows the whole isothermal magnetization cycle obtained for Co-5% at different temperatures (5, 15, and 25 K). Steps in the magnetization upturn can only be found at 5 K, as reported before.^{14–18} Interestingly enough, it can be appreciated that steps are only present in the first magnetization curve while they are absent in the negative side of the cycle: changes induced in the compound during these steps do not disappear when releasing the field, but are permanent. First magnetization curves recorded at 15 K and 25 K do not present steps, instead just show a smooth evolution of the magnetization. In spite of this, magnetization curves recorded at 15 K and 20 K have important similarities with the one of 5 K. First of all these curves present a high irreversibility between the switch on (first magnetization curve) and the release of the magnetic field. Second of all and more remarkable, as can be seen in Fig. 3(b), the curves of first magnetization (at the three temperatures) are out of the hysteresis cycle. In fact, the cycle after the first magnetization is quite thin, with a quite low remanence ($\sim 0.3 \mu_B/\text{Mn}$) and a coercive field (~ 325 Oe) that poorly depend on temperature [see inset of Fig. 3(b)]. This evidences that the effect of applying a magnetic field is the induction of an irreversible transition in this temperature region that cannot be ascribed to the apparition of steps in the $M(H)$ and $\rho(H)$ curves. This irreversible change under field reflects a continuous growth

of the FM component in the phase-separated phase. It is just at very low temperature ($T < 7$ K) that this transition takes place by means of abrupt steps.

These last observations establish clear differences between the present case and the austenite to martensite transformation under applied stress that also takes place through avalanches.^{23,24} In this last case, the austenite phase is recovered after releasing the stress and, in addition, avalanches are recovered when cycling stress induces the transition several times.²³ In fact, the initial austenite phase is more symmetric (cubic) than the final martensite phase (typically monoclinic or closed packed with many variants), while the contrary applies in the present case when the CO phase is less symmetric than the metallic one.

B. Neutron and synchrotron x-ray diffraction

Neutron and synchrotron x-ray powder diffraction data were collected at different temperatures for both Co-2% and Co-5% compounds. Both exhibit at RT the same $Pnma$ space group (SG) as the pristine compound. Figures 4(a) and 4(b) show the RT patterns (x-ray) for Co-2% and Co-5% respectively, refined using a single phase $Pnma$ structure ($\chi^2 = 2.94$, $R_B = 2.13$ for Co-2%, and $\chi^2 = 4.15$, $R_B = 2.51$ for Co-5%). Selected structural parameters, including interatomic distances and angles are given in Table I as obtained from combined refinements of high-resolution neutron and synchrotron data. Due to the slight amount of Co substitution the differences in the structural features are very tiny and in most cases are within the experimental error. The cell vol-

TABLE I. Structural details obtained at RT from combined refinements of neutron and synchrotron data. The cell distortion ($\xi \equiv 1000 \times [\frac{a+c}{b\sqrt{2}} - 1]$), Mn-O bond distances, and Mn-O-Mn bond angles, and strain parameters are also given.

	$\text{Pr}_{0.5}\text{Ca}_{0.5}\text{Mn}_{0.98}\text{Co}_{0.02}\text{O}_3$	$\text{Pr}_{0.5}\text{Ca}_{0.5}\text{Mn}_{0.95}\text{Co}_{0.05}\text{O}_3$
a (Å)	5.4023(1)	5.4031(1)
b (Å)	7.6126(2)	7.6144(2)
c (Å)	5.3929(1)	5.3936(1)
V (Å ³)	221.78(1)	221.90(1)
ξ	3	3
R_{Bragg} (%)	1.8	2.5
R_F (%)	2.5	3.1
χ^2	2.5	4.2
$\langle d_{\text{Mn-O}} \rangle$ (Å)	1.942(5)	1.942(5)
$\theta_{\text{Mn-O}(1)\text{-Mn}}$ (°)	158.1 (1)	158.3(1)
$\theta_{\text{Mn-O}(2)\text{-Mn}}$ (°)	158.1(6)	158.1(5)
Strain parameters		
S_{400}	0.168	0.174
S_{040}	0.089	0.087
S_{004}	0.143	0.148
S_{220}	-0.097	-0.058
S_{202}	0.772	0.743
S_{022}	-0.092	-0.054

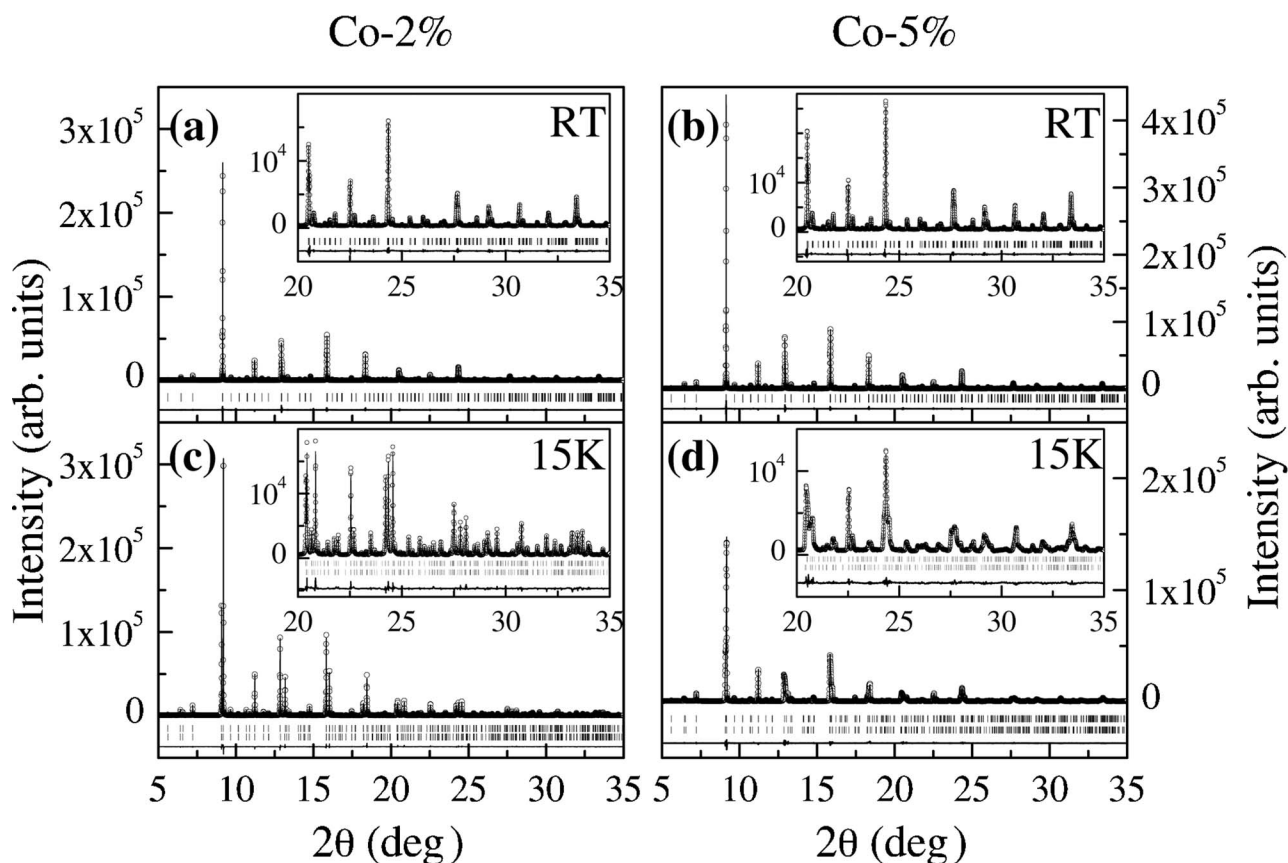


FIG. 4. Observed (circles), calculated, and difference SPD patterns ($\lambda=0.429\ 697\ \text{\AA}$) for (a) and (c) Co-2% at RT and 15 K respectively; (b) and (d) Co-5% at RT and 15 K, respectively. RT data were refined with a single $Pnma$ phase while 15 K data with two $Pnma$ phases (synchrotron x-ray data).

ume increases by the insertion of Co. Probably, according to the tiny volume gain, mean octahedra at Co sites are slightly more expanded than at Mn sites. The b axis manifests the larger change upon Mn substitution by Co, whereas the change in a and c parameters are comparatively smaller.

The evolution observed on cooling the samples below $T_{CO} \approx 240\ \text{K}$ revealed phase segregation into two types of mesoscopic domains. The transformation takes place between 200 and 240 K. The occurrence of phase segregation is illustrated in Fig. 5, where the same selected region of the refined SPD x-ray patterns is depicted at RT and 15 K for Co-2% [Figs. 5(a) and 5(c)], and for Co-5% sample [Figs. 5(b) and 5(d)]. In addition to the total calculated profile, at low temperature, the contribution to the spectra from each segregated phase is shown separately in Figs. 5(c) and 5(d). This figure shows mesoscopic phase separation and large coherent diffraction domains in both samples. It also reveals deep differences in the cell distortion of the separated phases in the Co-5% sample. This is in contrast with the Co-2% sample, which consists of two phases with rather similar angular distance between (202) and (040) reflections.

Refinements of the full SPD patterns (x ray) taken at 15 K were satisfactory with two segregated phases and are shown in Figs. 4(c) and 4(d) for Co-2% and Co-5%, respectively. Main results, and reliability factors, of the low temperature structural refinements are given in Table II (from x ray). This table gathers the cell dimensions determined for the different

phases and the refined weight fractions for the two compounds at 15 K (values for $\text{Pr}_{0.5}\text{Ca}_{0.5}\text{MnO}_3$ at 15 K are also given for comparison). The temperature evolution of cell parameters and phase fractions are presented in Fig. 6(a) for Co-2% and 6(b) for Co-5%.

1. $\text{Pr}_{0.5}\text{Ca}_{0.5}\text{Mn}_{0.98}\text{Co}_{0.02}\text{O}_3$

At 300 K (above $T_{CO} \approx 240\ \text{K}$) SPD patterns (x ray) present very symmetric single peaks signaling a single phased material. They transform in slightly asymmetric peaks at low temperature evidencing segregation of distinct mesoscopic domains. The Co-2% sample splits into two types of structures that exhibit the characteristic lattice deformation of the CO/OO state. Compared with the high temperature phase, both present a large compression of b and expanded a and c lattice parameters (Fig. 6). In Table I the ξ parameter expresses the difference between $b/\sqrt{2}$ and $(a+c)/2$ ($\xi \equiv 1000 \times \left[\frac{(a+c)}{b\sqrt{2}} - 1 \right]$). The two lattices of Co-2% are so similarly deformed that there is almost no difference in ξ (25 and 23). The small differences in cell dimensions could be unambiguously detected thanks to the very high angular resolution of the synchrotron x-ray data (the peak width due to the instrumental contribution is calculated to be $\approx 0.0007^\circ$ neglecting the broadening due to the axial divergence). The inset of Fig. 6 displays the temperature dependence of the relative fraction of each phase. The evolution is

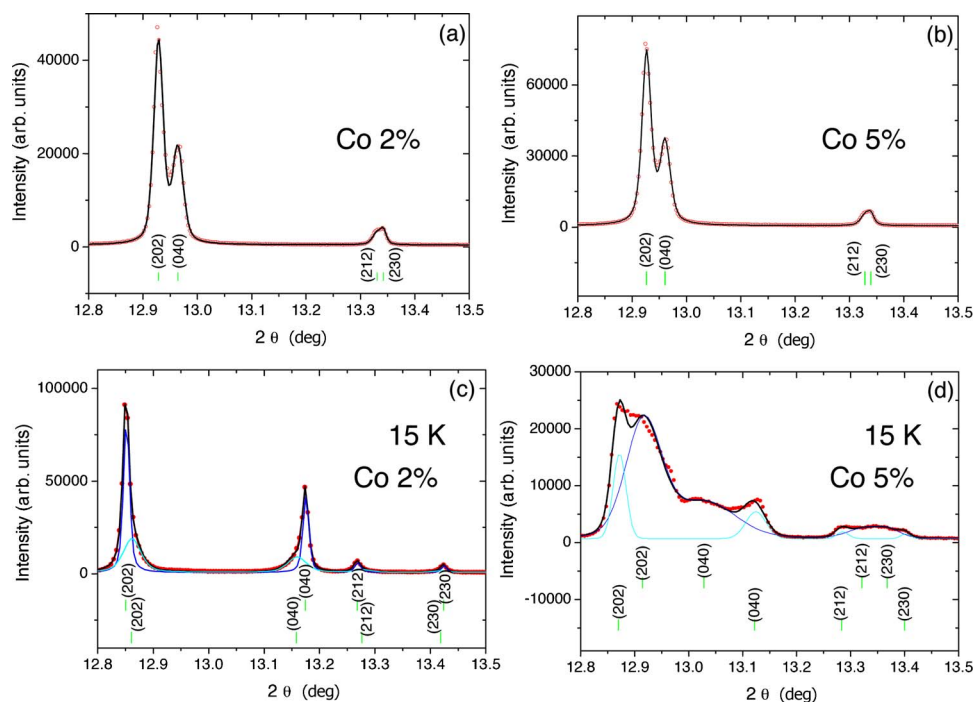


FIG. 5. (Color online): Selected region of the SPD ($\lambda=0.429\ 697\ \text{\AA}$) Rietveld refinements evidencing the phase segregation. (a) and (b) show RT data of Co-2% and Co-5%, respectively; (c) and (d) show data at 15 K (with two phases) of Co-2% and Co-5%, respectively. The separation of two phases with very tiny [large] differences in their cell dimensions is observed for Co-2% [Co-5%] sample (synchrotron x-ray data). Light/dark blue colors (color online) in (c) and (d) are calculations for, respectively, phase 1 and phase 2 in Table II.

monotonous below T_{CO} and reaches the equilibrium values around $T \approx 100\ \text{K}$: to yield $\sim 58\%$ (phase 1) and $\sim 42\%$ (phase 2).

The neutron diagram was refined using a single structural phase. NPD data show the presence at low temperatures of only one type of long-range magnetic order. Only CE-type magnetic ordering (with FM zigzag chains AFM coupled) was detected in the low temperature neutron diffraction patterns. Although the high-resolution D2B instrument was used, only one magnetic cell can be distinguished, compatible with the two lattices detected with x rays. As a first trial, we have refined NPD data by assuming that both phases are equally ordered. This renders an ordered magnetic moment of $2.0(1)\ \mu_B/\text{Mn}$ (maximum expected value: $3.5\ \mu_B/\text{Mn}$). Figure 7(a) shows the low angle region of the neutron pattern at 3 K with the main magnetic peaks refined and using the structural phases determined from SPD (undistinguishable in neutron data). As a second trial, we have assumed that just the majority phase (the most distorted) presents CE magnetic order. The ordered magnetic moment obtained is $2.8(2)\ \mu_B/\text{Mn}$. Both scenarios are possible. The most likely is that phases 1 and 2 which present only slightly different cell distortions both have CE-type magnetic order. Less probable is the case that only one of the phases exhibits long range magnetic order. In this second case the other phase would present a frozen (disordered) or short-range ordered magnetic state. This would allow that the magnetization steps in Fig. 3 correspond to the magnetization of disordered (or short range ordered) regions instead of the transition from a long range CE to a FM arrangement. In our opinion, there is evidence indicating that both phases present CE spin ar-

rangement and partial magnetic disorder. Both exhibit apically compressed MnO_6 octahedra with very similar lattice distortion ($\xi \approx 23-25$). Moreover, a sudden decrease of the CE magnetic signal has been reported coinciding with the avalanches.¹⁷

We recall that other works also report phase coexistence between similarly distorted phases in Al or Ga substituted manganites.^{12,25,26} But it must be highlighted that these substitutions do not generate FM even for higher contents as Co does.¹³ In addition, differing from the present case, this coexistence is accompanied by the presence of two AFM phases: CE and pseudo-CE.¹²

2. $\text{Pr}_{0.5}\text{Ca}_{0.5}\text{Mn}_{0.95}\text{Co}_{0.05}\text{O}_3$

The Co-5% sample displays qualitatively different features on cooling, as for instance the two phases segregated in $\text{Pr}_{0.5}\text{Ca}_{0.5}\text{Mn}_{0.95}\text{Co}_{0.05}\text{O}_3$ exhibit very different cells. This has also been found for other substituting cations inducing FM such as Cr.²⁷ The majority phase (82%) does not display the anisotropic lattice distortion of the secondary phase (18%). Inspection of the magnetic intensities in the low-angle region of the ND pattern taken at 5 K [Fig. 7(b)] revealed two sets of magnetic reflections [one of them is hardly visible, see inset in Fig. 7(b)]. Their indexation confirmed the coexistence of long-range ferromagnetism and traces of CE-type magnetic order, but no signal of pseudo-CE order as commonly found with other substituting ions such as Ni.¹⁸ The two ordered magnetic phases were observable below, respectively, $\approx 80\ \text{K}$ and $\approx 60\ \text{K}$. The refinement [Fig. 7(b)] was performed including these two magnetic phases. We have to emphasize that a very large ferromagnetic contribution

TABLE II. Cell parameters and phase fraction for 15 K coexisting phases (from x-ray data). The cell distortions (ξ , see Table I caption), Mn-O bond distances, and Mn-O-Mn bond angles, and strain parameters are also printed. Values corresponding to the pure $\text{Pr}_{0.5}\text{Ca}_{0.5}\text{MnO}_3$ compound are included for comparison.

	$\text{Pr}_{0.5}\text{Ca}_{0.5}\text{MnO}_3$	$\text{Pr}_{0.5}\text{Ca}_{0.5}\text{Mn}_{0.98}\text{Co}_{0.02}\text{O}_3$		$\text{Pr}_{0.5}\text{Ca}_{0.5}\text{Mn}_{0.95}\text{Co}_{0.05}\text{O}_3$	
		Phase 1	Phase 2	Phase 1	Phase 2
a (Å)	5.4362(2)	5.4321(1)	5.4288(3)	5.4102(1)	5.4269(1)
b (Å)	7.4828(3)	7.4915(2)	7.5006(5)	7.5745(2)	7.5206(2)
c (Å)	5.4339(2)	5.4282(1)	5.4231(3)	5.3957(1)	5.4165(1)
V (Å ³)	221.04(4)	220.90(1)	220.83(5)	221.17(1)	221.12(1)
ξ	27	25	23	9	20
Fraction	100%	58%	42%	82%	18%
R_{Bragg} (%)	4.6	3.0	3.1	2.5	3.3
R_F (%)	5.2	3.1	3.4	3.7	2.8
χ^2	2.2	6.5		2.8	
$d_{\text{Mn-O}(1)}$ (Å)	1.911(6)	1.901(6)	1.919(6)	1.933(4)	1.93(1)
$\langle d_{\text{Mn-O}(2)} \rangle$ (Å)	1.96(1)	1.95(1)	1.95(1)	1.94(1)	1.95(2)
$\theta_{\text{Mn-O}(1)\text{-Mn}}$ (°)	156.5(1)	157.4(1)	156.5(1)	156.9(1)	157.8(3)
$\theta_{\text{Mn-O}(2)\text{-Mn}}$ (°)	158.0(4)	158.0(6)	158.4(6)	157.6(5)	157(1)
Strain parameters					
S_{400}	0.118	0.087	0.496	2.230	0.306
S_{040}	0.027	0.025	0.291	2.653	0.247
S_{004}	0.188	0.089	1.114	2.975	0.329
S_{220}	0.078	0.062	0.532	-3.865	-0.226
S_{202}	0.383	0.225	2.318	9.177	0.872
S_{022}	-0.031	0.045	0.435	-4.710	-0.360

(structural phase 1) contrasts with a very weak AFM signal (from structural phase 2) in the diffraction pattern. In fact the relative intensity of the two observed magnetic phases is even smaller than expected from the low proportion of the secondary phase detected in SXD data. Ferromagnetism must be attributed to the nondistorted majority phase (82%), whereas the residual distorted, CO phase (18%) exhibits CE-type magnetic order. Assuming these concentrations for the two magnetic phases (under the hypothesis that they occupy different regions), we have refined the average ordered moment in the two types of magnetic domains: at 5 K we found 1.66(3) μ_B/Mn site in the ferromagnetic regions and 0.47(8) μ_B/Mn in the CO domains. The ferromagnetic intensity in the neutron pattern was satisfactorily reproduced with the ferromagnetic moments aligned parallel to the [010] direction (parallel to the b axis), whereas the components of the CE-type magnetic order are contained in the a - c plane. The ferromagnetic component in the whole sample deduced by assuming a 82% of ferromagnetic regions with 1.66(3) μ_B/Mn , 1.33(3) μ_B/Mn , is smaller than the low temperature magnetization deduced from Fig. 3(a) before the first induced field transition at ≈ 1.5 T [1.81(5) μ_B/Mn]. We ascribe this difference to a ferromagnetic component induced by the applied field below the first transition in measurements displayed in Fig. 3(a). The obtained values of the ordered magnetic moment clearly indicate that a large amount of magnetic moment remains disordered or just short-range ordered at low temperature. This would be in accordance

with the existence of a phase without long range magnetic order in Co-2%.

The analysis of the peak widths of the separated phases can also provide additional microstructural information. The Williamson-Hall plot of the peak widths [refined at 15 K from high resolution SPD data (x ray)] as a function of scattering vector for some families of peaks has been depicted in Fig. 8. Four classes of reflections are shown in this figure, where open and closed symbols correspond, respectively, to the majority and minority phases. Values in the figure were taken from the calculated powder diffraction profile. The Williamson-Hall approach relates the peak widths ($\Gamma_{\text{FWHM}} \approx \Gamma^{\text{Sample}} + \Gamma^{\text{Instr}} \approx \Gamma^{\text{Sample}}$, the instrumental broadening can be ignored in the present case) to the mean coherent diffraction domains [L (Å)] and the distribution ($\sigma = \Delta d$) of d spacings [$\Delta d/d$] for a selected class of reflections through the equation $\beta^* \cos(\theta) = (K\lambda/L) + 2(\Delta d/d)\sin(\theta)$, (K is a shape factor close to unity and β^* is the integral peak breadth, a measure of Γ_{FWHM} obtained through the ratio between the integrated intensity and the maximum intensity of the peak).

Several conclusions can be drawn from Fig. 8. There is a strong contrast between the degree of anisotropic strain in the majority phase of both compounds. The majority CE regions of Co-2% (phase 1) are characterized by a highly isotropic strain (all different families of peaks collapse to give a single line). On the contrary, the strain is highly anisotropic in the ferromagnetic domains of Co-5%. Very remarkable is a much wider distribution of d spacings for the families of

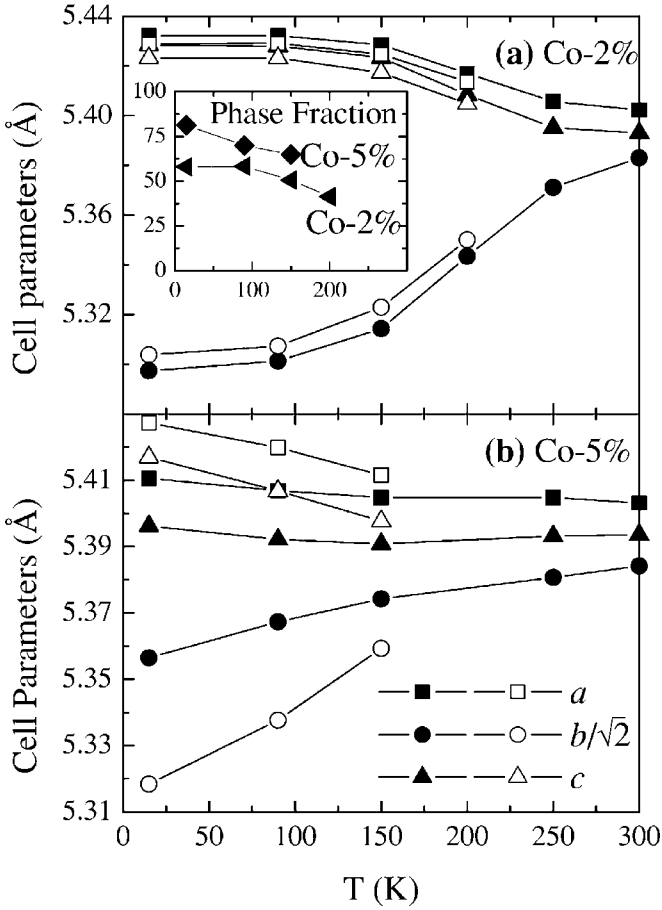


FIG. 6. Thermal evolution of lattice parameters for phase 1 (filled symbols) and phase 2 (open symbols) found by Rietveld refinement of SPD (x ray) data of (a) $\text{Pr}_{0.5}\text{Ca}_{0.5}\text{Mn}_{0.98}\text{Co}_{0.02}\text{O}_3$ and (b) $\text{Pr}_{0.5}\text{Ca}_{0.5}\text{Mn}_{0.95}\text{Co}_{0.05}\text{O}_3$. The inset shows the fraction of phase 1 (left triangles correspond to Co-2% and diamonds to Co-5%).

planes $(0k0)$ and $(h0h)$ (we recall that the strain of both is correlated due to twinning effects). No significant differences were observed in the volume averaged coherent scattering lengths for the different phases (of the order of a thousand of angstroms). Figure 8(b) and the strain parameters given in Table II establish that the ferromagnetic majority phase in the Co-5% sample is a strongly strained phase. A key structural difference between the FM/metallic and AFM/CO phases in manganites is the apical compression of the octahedra in the latter (responsible for the rising of $\xi \equiv (10^3 \times [\frac{a+c}{b\sqrt{2}} - 1])$). The average $\langle \xi \rangle$ value observed in the FM phase is $\langle \xi \rangle = 9$ (Table II), clearly much lower than in the CO phase, but still higher than in the RT structure. Figure 8 indicates that there exists a strong deviation of local ξ values in the unit cells within the FM regions with respect to the mean apical distortion $\langle \xi \rangle$. Locally, a significant continuous distribution $\Delta \xi$ in the apical compression of the octahedra would explain the anomalous broadening of $(0k0)$ and $(h0h)$ families of peaks in the FM defective phase [Fig. 8(b)]. Microstrains due to structural defects such as dislocations, stacking faults, etc related with the presence of Co ions also can contribute to the distribution of d spacings.

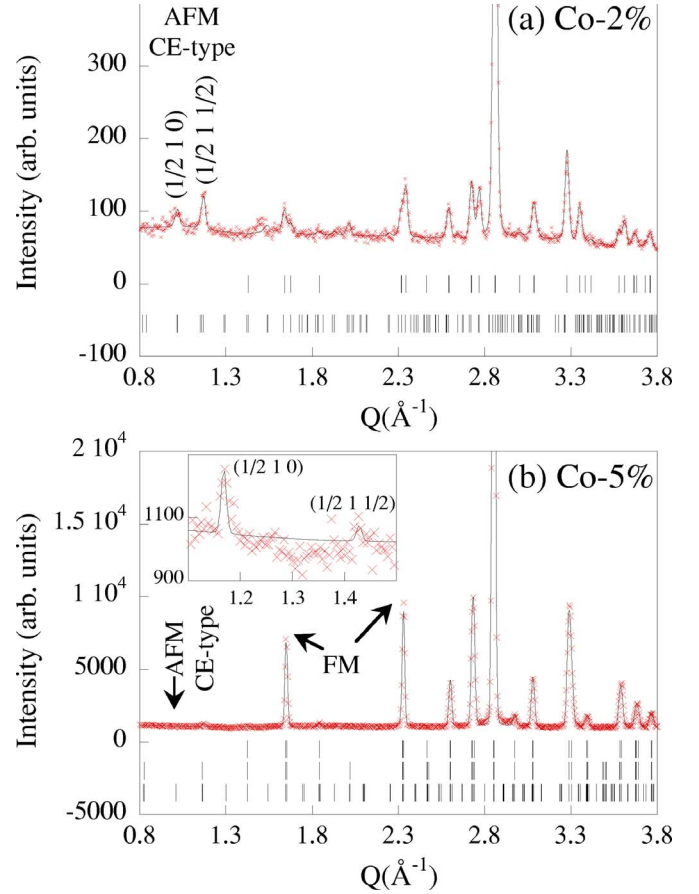


FIG. 7. (Color online): Neutron data. (a) $\text{Pr}_{0.5}\text{Ca}_{0.5}\text{Mn}_{0.98}\text{Co}_{0.02}\text{O}_3$: Low angle region of the refined neutron pattern ($\lambda = 1.594 \text{ \AA}$) at 3 K using a single structural phase and a CE-type magnetic model. (b) $\text{Pr}_{0.5}\text{Ca}_{0.5}\text{Mn}_{0.95}\text{Co}_{0.05}\text{O}_3$: Low angle region of the refined neutron pattern at 5 K ($\lambda = 2.426 \text{ \AA}$). First row of bars is the structural phase (the two phases are undistinguishable in neutron data). The second and third rows of bars correspond, respectively, to the ferromagnetic and the CE-type magnetic phases. The inset shows in detail the region where (very) small AFM CE-type peaks are observed.

IV. SUMMARY AND CONCLUSIONS

We studied the low temperature phase segregation of $\text{Pr}_{0.5}\text{Ca}_{0.5}\text{Mn}_{1-x}\text{Co}_x\text{O}_3$ ($x = 0.02$ and 0.05) compounds by means of magnetization and magnetotransport measurements, SPD and NPD. Results presented allow us to draw a picture of the evolution under Co substitution of the intrinsic microscopic inhomogeneities in this family. Our findings confirm a significant degree of complexity in these apparently simple materials. We highlight that, under just a 2% of Co substitution, two defective AFM/CE-type phases separated with 58/42 ratio, a very similar proportion. These phases present very similar structural distortions and magnetic properties. Just the CE type long-range magnetic arrangement is found at low T . The value of the ordered magnetic moment found, $2.0(1) \mu_B/\text{Mn}$, signals the presence of partial magnetic disorder due to the presence of Co, mainly in the minority phase. We have not detected spontaneously ordered ferromagnetic domains down to low temperatures.

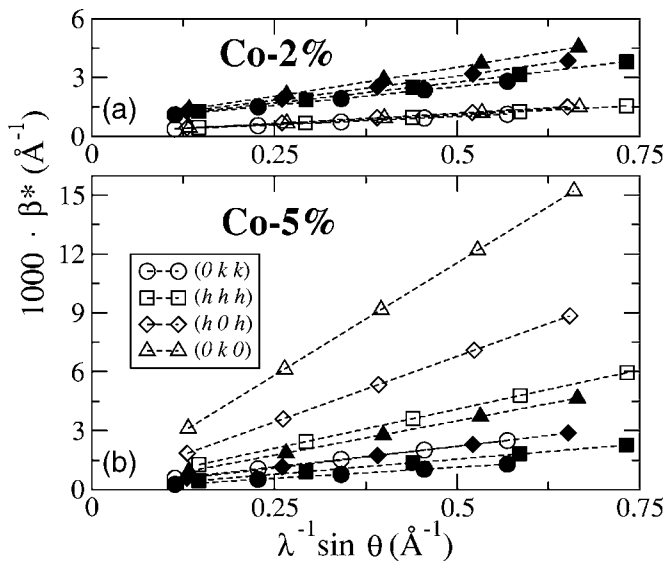


FIG. 8. Williamson-Hall plots of some families of peaks from SPD at 15 K for the segregated phases of (a) Co-2% and (b) Co-5% (x-ray data). Open and closed symbols correspond to the majority and minority phase, respectively.

On the contrary, under further substitution (Co-5%) a ferromagnetic phase develops and becomes clearly dominant (82% compared to 18% of the remaining phase). Neutron data show that the ordered magnetic moment of the ferromagnetic phase is well below the expected value [we find 1.66(3) instead of $3.5 \mu_B/\text{Mn}$]. The secondary phase is essentially magnetically disordered, although a CE magnetic structure with quite low ordered moment [$0.47(8) \mu_B/\text{Mn}$] is formed. Both the magnetic disorder and cell dimensions/distortion confirm us the similarity of this phase with the separated phases in the Co-2% compound. From the microstructural point of view, the internal strains increase with Co

substitution. In addition they are found to be stronger and much more anisotropic in the FM phase of the Co-5% ceramic sample. The observation of an anomalous broadening of mainly $(0k0)$ and $(h0h)$ families of peaks in the FM phase can be attributed to a wide distribution in the apical compression of the Mn/Co octahedra at a local level. The role of these strains in stabilizing the FM phase and in the depolarization of Mn moments must be further investigated.

Concerning magnetization and resistivity steps under field, they are present at low temperature ($T=5$ K) for both Co concentrations (2% and 5%) independently of the preexistence of a spontaneous ferromagnetic phase. We find that this phenomenon is highly irreversible and that the switch off of the magnetic field (after the occurrence of the steps) does not drive to the initial state but some permanent changes in the system remain (see also Ref. 13). In fact, after the first magnetization curve, the hysteresis cycles are smooth and quite thin (the resulting ferromagnetic state is soft). This behavior is independent of the occurrence of steps in the first magnetization curve and is also present at higher temperatures (up to 25 K). So, we conclude that the irreversibility of the magnetization process is independent of the occurrence of steps in the magnetization curve. Steps are one (very) special manifestation of this irreversible field induced changes.

ACKNOWLEDGMENTS

Financial support by the MEC (MAT2003-07483-C02-02) and Generalitat de Catalunya (2005-GRQ-00509, PICS2005-14) is gratefully acknowledged. C.F. acknowledges financial support from MEC (Spain). The FAME European Network of Excellence is also acknowledged. We thank LLB, ILL, and ESRF for the provision of beam time. The authors acknowledge fruitful discussions with Ll. Mañosa, E. Vives, and J. Ortín.

- ¹J. M. Tranquada, B. J. Sternlieb, J. D. Axe, Y. Nakamura, and S. Ishida, *Nature (London)* **375**, 561 (1995); H. A. Mook and F. Dogan, *ibid.* **401**, 145 (1999).
- ²Y. Moritomo, Y. Tomioka, A. Asamitsu, Y. Tokura, and Y. Matsui, *Phys. Rev. B* **51**, 3297 (1995); S. Mori, C. H. Chen, and S.-W. Cheong, *Nature (London)* **392**, 473 (1998).
- ³J. B. Goodenough, *Phys. Rev.* **100**, 564 (1955).
- ⁴P. Radaelli, D. E. Cox, M. Marezio, and S.-W. Cheong, *Phys. Rev. B* **55**, 3015 (1997).
- ⁵J. García, M. C. Sánchez, J. Blasco, G. Subías, and M. G. Proietti, *J. Phys.: Condens. Matter* **13**, 3243 (2001).
- ⁶S. Grenier, J. P. Hill, D. Gibbs, K. J. Thomas, M. v. Zimmerman, C. S. Nelson, V. Kiryukhin, Y. Tokura, Y. Tomioka, D. Casa, T. Gog, and C. Venkataraman, *Phys. Rev. B* **69**, 134419 (2004).
- ⁷J. Herrero-Martín, J. García, G. Subías, J. Blasco, and M. Concepcion Sánchez, *Phys. Rev. B* **70**, 024408 (2004).
- ⁸R. J. Goff and J. P. Attfield, *Phys. Rev. B* **70**, 140404(R) (2004).
- ⁹A. Daoud-Aladine, J. Rodríguez-Carvajal, L. Pinsard-Gaudart, M. T. Fernández-Díaz, and A. Revcolevschi, *Phys. Rev. Lett.* **89**,

097205 (2002).

- ¹⁰S. Laroche, A. Mehta, N. Kaneko, K. Mang, A. F. Panchula, L. Zhou, J. Arthur, and M. Greven, *Phys. Rev. Lett.* **87**, 095502 (2001).
- ¹¹K. Takenaka, S. Okuyama, R. Shiozaki, T. Fujita, and S. Sugai, *J. Appl. Phys.* **91**, 294 (2002). T. Katsufuji, S.-W. Cheong, S. Mori, and C.-H. Chen, *J. Phys. Soc. Jpn.* **68**, 1090 (1999); A. Machida, Y. Moritomo, E. Nishibori, M. Takata, M. Sakata, K. Ohoyama, S. Mori, N. Yamamoto, and A. Nakamura, *ibid.* **69**, 3536 (2000).
- ¹²C. Martin, A. Maignan, F. Damay, M. Hervieu, B. Raveau, Z. Jirak, G. André, and F. Bourée, *J. Magn. Magn. Mater.* **202**, 11 (1999).
- ¹³S. Hébert, A. Maignan, and C. Martin, *B. Raveau, Solid State Commun.* **121**, 229 (2002).
- ¹⁴S. Hébert, A. Maignan, V. Hardy, C. Martin, M. Hervieu, B. Raveau, R. F. Mahendiran, and P. Schiffer, *Eur. Phys. J. B* **29**, 419 (2002).
- ¹⁵R. Mahendiran, A. Maignan, S. Hébert, C. Martin, M. Hervieu, B.

- Raveau, and J. F. Mitchell, P. Schiffer, *Phys. Rev. Lett.* **89**, 286602 (2002).
- ¹⁶S. Hébert, V. Hardy, A. Maignan, R. Mahendiran, M. Hervieu, C. Martin, and B. Raveau, *J. Solid State Chem.* **165**, 6 (2002).
- ¹⁷C. Yaicle, C. Martin, Z. Jirak, F. Fauth, G. André, E. Suard, A. Maignan, V. Hardy, R. Retoux, M. Hervieu, S. Hébert, B. Raveau, C. Simon, D. Saurel, A. Brûlet, and F. Bourée, *Phys. Rev. B* **68**, 224412 (2003).
- ¹⁸J. L. Garcia-Muñoz, N. Bellido, C. Frontera, J. Hernández-Velasco, C. Ritter, C. Yaicle, C. Martin, and A. Maignan, *J. Appl. Phys.* **97**, 10H701 (2005).
- ¹⁹J. Rodríguez-Carvajal, *Physica B* **192**, 55 (1993).
- ²⁰O. Masson, E. Dooryhée, R. W. Cheary, and A. N. Fitch, *Mater. Sci. Forum* **378**, 300 (2001).
- ²¹P. W. Stephens, *J. Appl. Crystallogr.* **32**, 281 (1999). See also *An introduction to the program FullProf 2000*, by J. Rodríguez-Carvajal (included in the distribution of FullProf-Suite).
- ²²D. E. Cox, P. G. Radaelli, M. Marezio, and S.-W. Cheong, *Phys. Rev. B* **57**, 3305 (1998); C. Frontera, J. L. García-Muñoz, A. Llobet, M. Respaud, J. M. Broto, J. S. Lord, and A. Planes, *ibid.* **62**, 3381 (2000).
- ²³L. Carrillo and J. Ortín, *Phys. Rev. B* **56**, 11508 (1997).
- ²⁴V. Hardy, S. Majumdar, S. Crowe, M. R. Lees, D. McK. Paul, L. Hervé, A. Maignan, S. Hébert, C. Martin, C. Yaicle, M. Hervieu, and B. Raveau, *Phys. Rev. B* **69**, 020407(R) (2004).
- ²⁵C. Frontera, J. L. García-Muñoz, A. Llobet, M. A. G. Aranda, C. Ritter, M. Respaud, and J. Vanacken, *J. Phys.: Condens. Matter* **13**, 1071 (2001).
- ²⁶C. Yaicle, F. Fauth, C. Martin, R. Retoux, Z. Jirak, M. Hervieu, B. Raveau, and A. Maignan, *J. Solid State Chem.* **178**, 1652 (2005).
- ²⁷F. Damay, C. Martin, A. Maignan, M. Hervieu, and B. Raveau, *Appl. Phys. Lett.* **73**, 3772 (1998).